D-mannose suppresses oxidative response and blocks phagocytosis in experimental neuroinflammation

Jing Wang[a,b,c], Negin Jalali Motlagh[a,b], Cuihua Wang[a,b], Gregory R. Wojtkiewicz[b], Stephan Schmidt[b], Cindy Chau[a,b], Radha Narsimhan[a,b], Enrico G. Kuellenberg[a,b], Cindy Zhu[a,b], Jenny Linnoila[a], Zhenwei Yao[c,1], and John W. Chen[a,b,1]

[a]Department of Radiology, Institute for Innovation in Imaging, Massachusetts General Hospital, Harvard Medical School, Boston, MA 02114; [b]Center for Systems Biology, Massachusetts General Hospital, Harvard Medical School, Boston, MA 02114; and [c]Department of Radiology, Huashan Hospital, Fudan University, Shanghai 200040, China

Edited by Lawrence Steinman, Stanford University School of Medicine, Stanford, CA, and approved August 26, 2021 (received for review April 22, 2021)

Inflammation drives the pathology of many neurological diseases. D-mannose has been found to exert an antiinflammatory effect in peripheral diseases, but its effects on neuroinflammation and inflammatory cells in the central nervous system have not been studied. We aimed to determine the effects of D-mannose on key macrophage/microglial functions—oxidative stress and phagocytosis. In murine experimental autoimmune encephalomyelitis (EAE), we found D-mannose improved EAE symptoms compared to phosphate-buffered saline (PBS)-control mice, while other monosaccharides did not. Multiagent molecular MRI performed to assess oxidative stress (targeting myeloperoxidase [MPO] using MPO-bis-5-hydroxytryptamide diethylenetriaminepentaacetate gadolinium [Gd]) and phagocytosis (using cross-linked iron oxide [CLIO] nanoparticles) in vivo revealed that D-mannose–treated mice had smaller total MPO-Gd^+ areas than those of PBS-control mice, consistent with decreased MPO-mediated oxidative stress. Interestingly, D-mannose–treated mice exhibited markedly smaller $CLIO^+$ areas and much less T2 shortening effect in the $CLIO^+$ lesions compared to PBS-control mice, revealing that D-mannose partially blocked phagocytosis. In vitro experiments with different monosaccharides further confirmed that only D-mannose treatment blocked macrophage phagocytosis in a dose-dependent manner. As phagocytosis of myelin debris has been known to increase inflammation, decreasing phagocytosis could result in decreased activation of proinflammatory macrophages. Indeed, compared to PBS-control EAE mice, D-mannose–treated EAE mice exhibited significantly fewer infiltrating macrophages/activated microglia, among which proinflammatory macrophages/microglia were greatly reduced while antiinflammatory macrophages/microglia increased. By uncovering that D-mannose diminishes the proinflammatory response and boosts the antiinflammatory response, our findings suggest that D-mannose, an over-the-counter supplement with a high safety profile, may be a low-cost treatment option for neuroinflammatory diseases such as multiple sclerosis.

neuroinflammation | D-mannose | oxidative stress | phagocytosis | imaging

Multiple sclerosis (MS) is a devastating, chronic inflammatory disorder of the central nervous system (1). The innate immune response from macrophages (MΦ) and microglia (Mg) plays key roles in both pathogenesis and repair in MS (2). One of the hallmarks of MS is the phagocytosis of myelin debris by MΦ and Mg (3). These foamy phagocytes present antigens to autoreactive T cells (4, 5) and correlate with MS disease activity (6). These cells can release proinflammatory factors to drive MS progression (7, 8). However, these myeloid cells can also shift toward a reparative phenotype, clearing damage and releasing antiinflammatory factors to initiate repair (3, 9). Such a shift may be instigated by prolonged phagocytosis of myelin (10). However, current disease-modifying therapies do not directly target MΦ and Mg. Furthermore, these drugs are expensive and have risen in cost five to seven times faster than the rate of prescription drug inflation (11), causing some patients to skip needed doses or take drug holidays. Thus, there is growing interest in developing inexpensive therapies for neuroinflammation and MS, potentially by targeting the underexplored MΦ and Mg.

D-mannose is a simple hexose sugar used as a dietary supplement. It exists in certain fruits such as cranberries, apples, and blueberries. D-mannose has been used as a treatment for urinary tract infections due to its antiadhesive effect against bacteria (12, 13). Importantly, D-mannose also has antiinflammatory properties (14–18). For example, D-mannose treatment can inhibit the neutrophil oxidative burst by suppressing neutrophil oxidative metabolism (14) and attenuate the inflammatory reaction in wound healing (16). No similar effects were found for other hexose sugars such as glucose, galactose, or fructose (15–17). However, the effect of D-mannose on MΦ and Mg in neuroinflammation has not yet been explored.

One of the deleterious substances released by activated MΦ/Mg in MS is myeloperoxidase (MPO), a key mediator of oxidative stress that plays a role in damaging neurons, oligodendrocytes, and axons in the MS brain (19). MPO is an enzyme produced specifically in myeloid-lineage cells that catalyzes hydrogen peroxide to form hypochlorous acid and other reactive oxidants (20, 21). In MS, MPO is present in high quantities in active MS plaques, where it is secreted mainly by

Significance

The innate immune response from macrophages and microglia plays key roles in the pathogenesis and repair in neuroinflammatory diseases such as multiple sclerosis. However, current disease-modifying therapeutics do not directly target these cells. Moreover, current drugs are expensive, causing some patients to skip doses or take drug holidays. We found that D-mannose not only decreased oxidative stress and blocked phagocytosis but also diminished the proinflammatory response and boosted the antiinflammatory response from macrophages and microglia. Our findings suggest that D-mannose, an over-the-counter drug with a high safety profile, may be an effective, low-cost treatment option for multiple sclerosis and other neuroinflammatory diseases. The availability of such a drug could significantly improve patient access to needed drugs and improve outcome.

Author contributions: J.W., Z.Y., and J.W.C. designed research; J.W., N.J.M., C.W., G.R.W., S.S., C.C., R.N., E.G.K., C.Z., and J.L. performed research; C.W. contributed new reagents/analytic tools; J.W., N.J.M., E.G.K., C.Z., Z.Y., and J.W.C. analyzed data; and J.W., Z.Y., and J.W.C. wrote the paper.

The authors declare no competing interest.

This article is a PNAS Direct Submission.

[1]To whom correspondence may be addressed. Email: aocnhnr@126.com or jwchen@mgh.harvard.edu.

This article contains supporting information online at http://www.pnas.org/lookup/suppl/doi:10.1073/pnas.2107663118/-/DCSupplemental.

Published October 26, 2021.

MΦ/Mg within or around the plaques in response to inflammatory stimuli (19–21). Elevated MPO activity can damage both white and gray matter (22, 23). In addition, emerging evidence has revealed that MPO not only exerts damaging oxidative effects, but also functions as a potent modulator of cell signaling and cell–cell interactions to regulate inflammatory signaling cascades (24–27). MΦ exposed to MPO show increased secretion of proinflammatory cytokines, a process mediated via the macrophage mannose receptor (MMR, CD206) (26, 28–30). Interestingly, it has been reported that administration of D-mannose can attenuate MPO-mediated signaling by blocking MMR on the surface of MΦ (15, 28, 31, 32). Another key function of MΦ/Mg is phagocytosis. One of the key receptors in phagocytosis is also the MMR, for which D-mannose is a ligand. Phagocytosis via the MMR can stimulate the release of proinflammatory cytokines, including IL-1, TNF, and reactive oxygen intermediates, which can further enhance the clearance of antigens (33). Nevertheless, it is currently unknown how D-mannose administration will affect MPO-mediated oxidative stress and phagocytosis in vivo.

In this study, we aimed to observe how these key MΦ/Mg functions of oxidative stress and phagocytosis change in response to D-mannose administration in living animals induced with experimental autoimmune encephalomyelitis (EAE), a commonly used mouse model to study neuroinflammation and MS, and to determine whether D-mannose can improve outcome in neuroinflammation. We employed a multiagent molecular imaging approach. The MPO-activatable imaging agent MPO-bis-5-hydroxytryptamide diethylenetriaminepentaacetate gadolinium (Gd) can specifically detect lesions with MPO-mediated oxidative response on T1-weighted (T1W) MRI and reflects proinflammatory MΦ and Mg in the central nervous system (CNS) (19, 34–36). It thus allows tracking of MPO^+ cells to estimate the oxidative stress burden. The other MRI agents are iron oxide nanoparticles. These magnetic nanoparticles can be taken up by activated phagocytes in inflamed areas and detected on MRI by T2-weighted imaging (37–39). Thus, MPO-Gd and iron oxide nanoparticles can be used in combination to investigate MΦ/Mg functions in vivo.

Results

D-Mannose Improved EAE Symptoms and Decreased MPO-Mediated Oxidative Stress. D-mannose treatment resulted in improved survival: 10/12 (83%) mice survived in the D-mannose–treated group, while only 4/12 (33%) mice survived in the phosphate-buffered saline (PBS)-control group (Fig. 1*A*, $P = 0.019$). Mice treated with D-mannose showed less severe clinical symptoms and lost less weight (Fig. 1 *B–C*, $n = 12$, $P < 0.001$ for clinical score, $P = 0.0023$ for weight). On the other hand, other monosaccharides, such as D-glucose, D-galactose, and D-fructose, did not improve clinical scores (*SI Appendix*, Fig. S1). To examine the effect D-mannose has on oxidative stress, on day 15 after induction, MPO-Gd MRI was performed. MPO-Gd imaging showed that D-mannose–treated mice had significantly smaller $MPO\text{-}Gd^+$ lesion areas ($P = 0.013$) compared to those of PBS-control mice ($n = 3$ in each group) (Fig. 1 *D–F*). These findings revealed that D-mannose attenuated MPO-mediated oxidative response in neuroinflammatory conditions.

D-Mannose Shifted Proinflammatory Response to an Antiinflammatory Response. To better understand the MPO-Gd MRI finding, we harvested spinal cords for flow cytometric analyses on day 19. We detected a significantly decreased percentage of infiltrating MΦ/activated Mg in D-mannose–treated mice compared to that of PBS-control mice ($P = 0.032$) (Fig. 2*C*). Correspondingly, fewer resident Mg were found in PBS-control EAE mice ($P = 0.011$) (Fig. 2*D*). Furthermore, we also found that D-mannose treatment increased the proportion of M2-like MΦ/Mg ($P = 0.034$), which are known to have MMR on their cell surface and exhibit antiinflammatory properties (Fig. 2*E*). Conversely, the spinal cords of PBS-control EAE mice contained abundant M1-like MΦ/Mg (Fig. 2*F*). After D-mannose treatment, M1-like MΦ/Mg decreased ($P = 0.0028$). These results suggested that D-mannose attenuated MPO-mediated proinflammatory response and increased M2-like MΦ/Mg, possibly to promote repair.

D-Mannose Decreased Phagocytosis In Vivo. We performed pre- and postcontrast T2-weighted imaging and T2 mapping experiments with CLIO to study phagocytosis. As CLIO shortens T2 relaxation time with little effect on T1 relaxation time, CLIO-enhanced lesions display lower signal intensity than unenhanced normal spinal cord on T2-weighted images (Fig. 3 *A* and *B*, red arrows). Significantly fewer $CLIO^+$ lesions were found in the spinal cords of D-mannose–treated mice as compared to those in PBS-control mice ($P < 0.0001$, Fig. 3*C*). The mean T2 values of the $CLIO^+$ lesions in the PBS-control group were also significantly lower than those in the D-mannose–treated group of mice ($P = 0.021$, Fig. 3*D*). These findings indicated that phagocytes in D-mannose–treated mice had taken up less CLIO than those in PBS-control mice. As expected, given that CLIO can be taken up by both activated M1-like and M2-like MΦ/Mg, whereas MPO is only expressed by activated M1-like MΦ/Mg (34, 39), the $CLIO^+$ lesion areas were larger than $MPO\text{-}Gd^+$ lesion areas in the PBS-control group ($P = 0.004$, Fig. 3*E*). However, in the D-mannose–treated group, we found that $CLIO^+$ areas trended smaller than $MPO\text{-}Gd^+$ areas ($P = 0.14$, Fig. 3*F*). Indeed, while most lesions matched between MPO-Gd and CLIO imaging in PBS-control EAE mice (Fig. 4*A*, white arrow), some lesions showed only CLIO signal without corresponding MPO-Gd signal (Fig. 4*A*, red arrow). On histology, areas that were positive for both MPO-Gd and CLIO on imaging were found to contain MPO-positive cells that did not express MMR (CD206), consistent with proinflammatory cells (Fig. 4*C*). In contrast, cells in areas that were negative for MPO-Gd but positive for CLIO showed virtually no MPO immunostaining but expressed CD206, revealing that these are antiinflammatory, M2-like cells (Fig. 4*D*). D-mannose treatment altered this dynamic, where most lesions are $MPO\text{-}Gd^+$ but there was very little $CLIO^+$ signal (Fig. 4*B*, yellow arrows), demonstrating a decreased phagocytic capacity of the MPO^+ inflammatory cells when treated with D-mannose.

D-Mannose Decreases Phagocytosis In Vitro. To confirm that D-mannose blocked phagocytosis, bone marrow–derived monocytes were differentiated and polarized to M1 and M2 MΦ. We used fluorescein isothiocyanate conjungated CLIO (FITC-CLIO) to assess the phagocytic capability of MΦ after incubating with different concentrations of D-mannose (0 mM, 1 mM, 10 mM, and 50 mM). We found that as we increased D-mannose concentration, the phagocytic capability of M1 and M2 MΦ significantly decreased compared to M0 MΦ ($P = 0.0025$ for M1, $P = 0.001$ for M2, Fig. 5). When M1 MΦ were treated similarly with D-glucose, D-galactose, or D-fructose, no change in phagocytosis levels was found (*SI Appendix*, Fig. S2). These results confirmed that only D-mannose decreased the ability of MΦ to phagocytose CLIO.

Discussion

Macrophage and microglia are key components of the innate immune response in the CNS. However, aberrant activation of these cells can drive the response toward damage and eventual neurodegeneration. In this study, we demonstrated that D-mannose, a widely available dietary supplement, improved clinical symptoms and reduced mortality in a murine neuroinflammation model. Observing MΦ/Mg functions using multiagent molecular

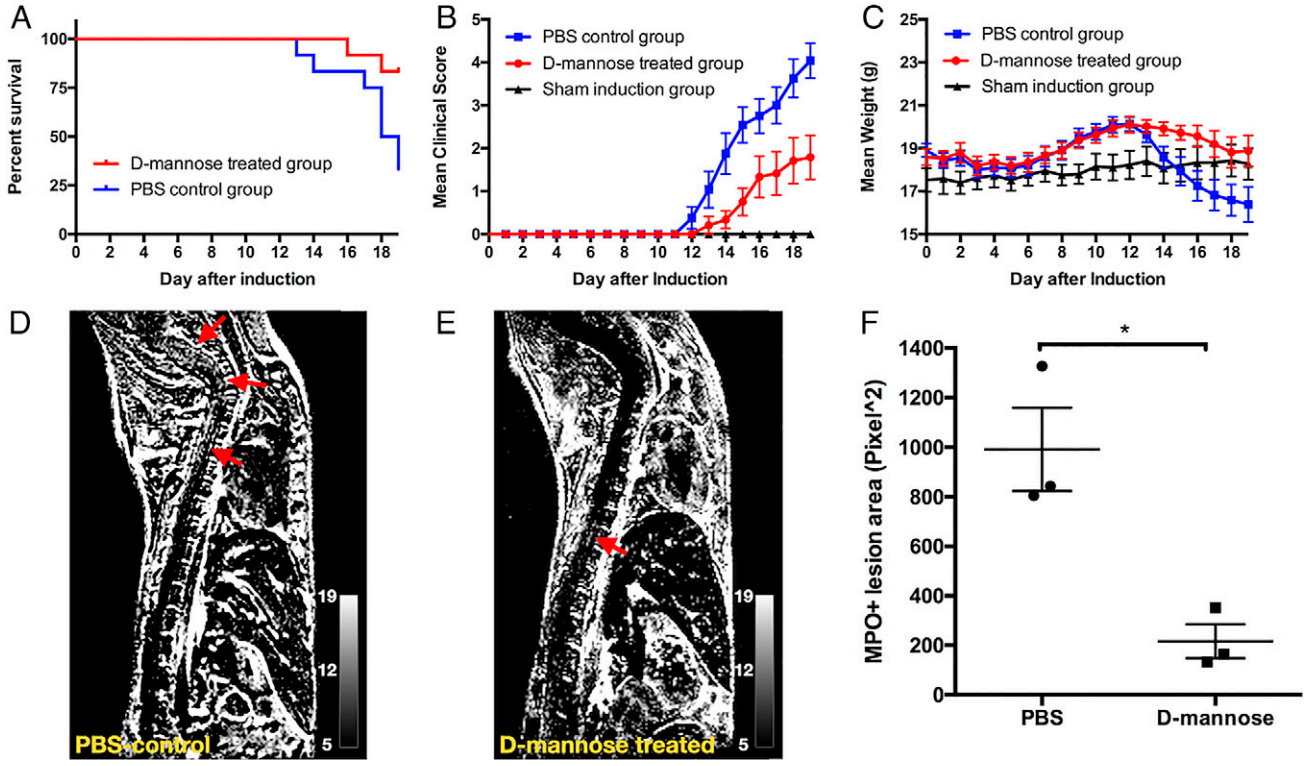

Fig. 1. D-mannose treatment improves clinical symptoms and alleviates inflammatory pathology. (*A*) Survival plot of D-mannose–treated mice and PBS-control mice with survival rates of 83 and 33%, respectively ($n = 12$, $P = 0.019$). (*B*) Clinical score and (*C*) daily weight of mice. Significant differences were found between the PBS-control and D-mannose–treated groups ($P < 0.001$ for clinical score, $P = 0.0023$ for weight). (*D* and *E*) Representative subtracted (postcontrast – precontrast) MPO-Gd enhanced T1-weighted images for (*D*) PBS-control and (*E*) D-mannose–treated mice, with arrows indicating the MPO^+ lesions. (*F*) Total lesion area was measured ($n = 3$) and D-mannose–treated mice showed significantly smaller lesion area than that of PBS-treated mice (*$P = 0.013$).

imaging, we found that D-mannose decreased MPO-mediated oxidative response and partially blocked MΦ/Mg phagocytosis in the CNS in living animals. We also showed that D-mannose treatment decreased infiltrating M1-like MΦ/Mg and boosted M2-like anti-inflammatory MΦ/Mg in inflamed tissues. These findings revealed that D-mannose administration decreases damaging MΦ/Mg inflammation and could shift the response toward repair. Other monosaccharides such as D-glucose, D-fructose, or D-galactose did not alter disease course or reduce phagocytosis.

Previous studies have suggested that MPO is a potent mediator of active inflammation and consequent demyelination in MS and EAE, secreted mainly by proinflammatory MΦ/Mg in response to inflammatory stimuli (19, 22, 23, 36). It has been reported that MΦ/Mg exposed to MPO show increased secretion of proinflammatory cytokines via the MMR (26, 28–30). The MMR is a 175-kDa transmembrane endocytic receptor that recognizes complex oligosaccharides terminating in mannose, fucose, or *N*-acetylglucosamine (40). It is involved in clearing endogenous molecules, promoting antigen presentation, triggering cytokine production, and modulating cellular activation (41). Compared to other oligosaccharides, D-mannose binds to MMRs with the highest affinity (42). Thus, D-mannose likely blocks MΦ/Mg phagocytosis by interacting with the mannose receptor on the MΦ/Mg.

Due to blood–brain barrier (BBB) breakdown, MΦ from the blood compartment migrate into the CNS parenchyma. Mg are the resident immunocompetent cells and are known as the "sensor for pathological events" in the CNS due to their responsiveness to a variety of pathological stimuli (43). Mg activated in response to inflammation and MΦ recruited through the damaged BBB are crucial mediators of tissue damage through several mechanisms, including the production of proinflammatory cytokines, matrix metalloproteinases, and free radicals (44, 45). Therefore, suppressing Mg activity or inducing infiltrating MΦ to polarize toward an antiinflammatory phenotype may help ameliorate MS/EAE. In this study, we found that D-mannose treatment not only reduced infiltrating MΦ and activated Mg, but also helped to retain more resident Mg compared to the PBS-control group. Among MΦ/Mg, EAE mice treated with D-mannose showed fewer MPO^+ MΦ/Mg, which mediate proinflammatory responses in the CNS. At the same time, more anti-inflammatory MΦ/Mg were found in the spinal cord. A possible mechanism for these results is the modulation of the MPO-mediated proinflammatory response by D-mannose via interaction with the MMR.

The balance between damage and repair caused by the innate immune system is key to understanding mechanisms of inflammatory lesion progression and resolution. We used a multiagent molecular MRI approach to examine two key MΦ/Mg functions. We found that MPO^+ lesions and $CLIO^+$ lesions did not always match. This is likely because, while MPO is predominately an M1 marker, phagocytosis can be performed by both M1- and M2-like MΦ/Mg. As such, we found a slightly higher lesion area on CLIO imaging compared to MPO imaging in PBS-control mice, reflecting differences in the cells involved in MPO production and phagocytosis. Correlating with histopathology, we were able to identify imaging appearances for different inflammatory cell phenotypes. Lesions that are MPO-Gd^+ and $CLIO^+$ reflect M1-like cells that are actively causing damage. Lesions that are only $CLIO^+$, without matching MPO-Gd^+ lesions, represent M2-like cells that are performing repair (Fig. 4 *A* and

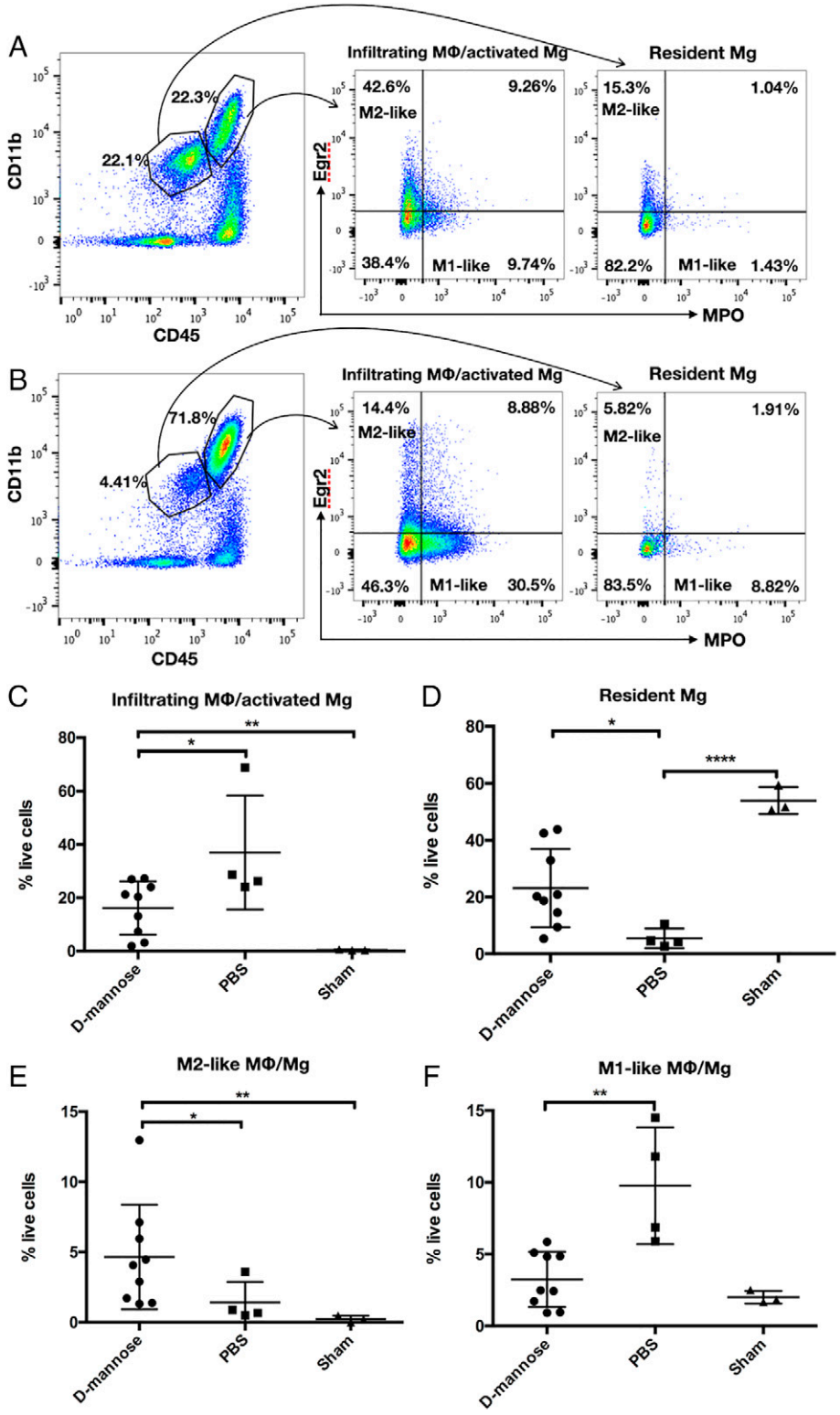

Fig. 2. D-mannose treatment decreases infiltrating MΦ/activated Mg and increases M2-like MΦ/Mg in spinal cord of EAE mice. Flow cytometry gating and representative plots for (*A*) D-mannose–treated mice and (*B*) PBS-control mice. Gating strategies are shown for identification of the respective leukocyte subsets and are used for all samples. (*C*) D-mannose–treated mice have significantly fewer infiltrating MΦ/activated Mg and (*D*) more resident Mg than those in PBS-control mice. (*E*) D-mannose–treated mice have more M2-like MΦ/Mg than that of PBS-control mice. (*F*) D-mannose–treated mice have fewer M1-like MΦ/Mg than that of PBS-control mice. $*P < 0.05$, $**P < 0.01$, $****P < 0.0001$.

B). Therefore, this multiagent imaging approach may allow us to identify the balance between damage and repair in neuroinflammation in vivo.

Foamy phagocytes that have phagocytosed myelin promote damage and MS progression (3). However, prolonged phagocytosis of myelin debris has been found to shift phagocytes to an

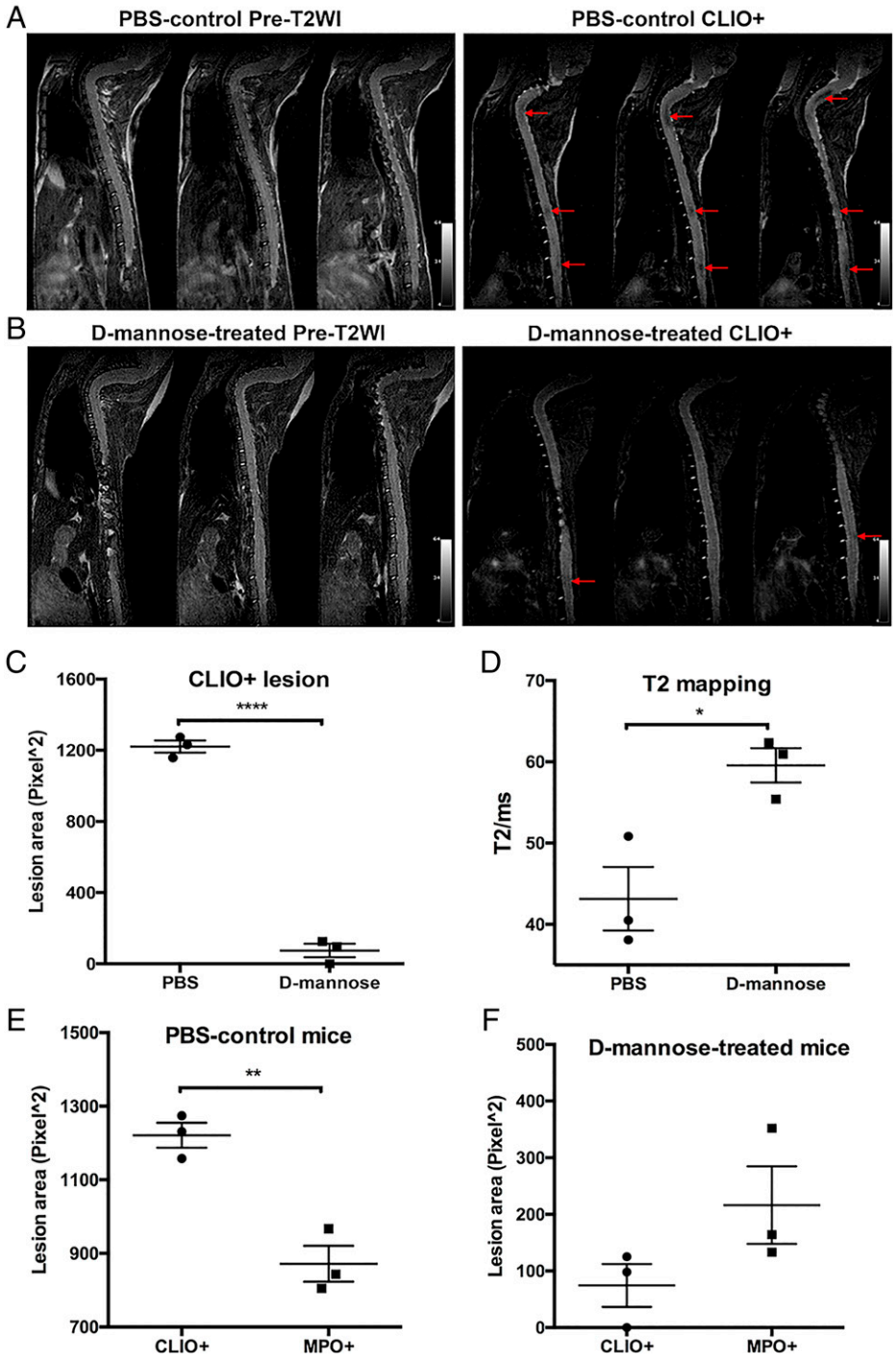

Fig. 3. Phagocytosis imaging and analyses with CLIO nanoparticles. Representative consecutive slices of pre- and postcontrast enhanced T2-weighted MR imaging of (*A*) PBS-control and (*B*) D-mannose–treated mice. Low signal $CLIO^+$ lesions (arrows) were found on postcontrast enhanced T2-weighted imaging in PBS-control mice and D-mannose–treated mice. (*C*) A significantly smaller total lesion area was found for D-mannose–treated mice than for PBS-control mice. (*D*) T2 values of the $CLIO^+$ lesions in the PBS-control group of mice were significantly lower than those in the D-mannose–treated group of mice. (*E*) In PBS-control mice, the mean $CLIO^+$ lesion area was larger than the mean MPO^+ lesion area, while (*F*) in D-mannose–treated mice, the mean $CLIO^+$ lesion area was smaller than the mean MPO^+ lesion area. $^*P < 0.05$, $^{**}P < 0.01$, $^{****}P < 0.0001$.

antiinflammatory phenotype (10). Thus, our finding that D-mannose partially blocked phagocytosis may serve to decrease the activation of the proinflammatory phenotype in these cells. At the same time, the dose of D-mannose we used did not result in complete blockage, so the phagocytes were still able to take up enough damaged myelin to shift the phenotype toward repair. Additionally, it has been reported that high concentrations of D-mannose can inhibit binding to the MMR, while low concentrations can enhance binding to the MMR (46). Future studies may be performed to optimize the dosage of D-mannose such that the balance between damage and repair shifts mostly toward repair.

D-mannose is widely used for the treatment of urinary tract infections (UTIs) with a dose of 2 g once to twice daily (12). For

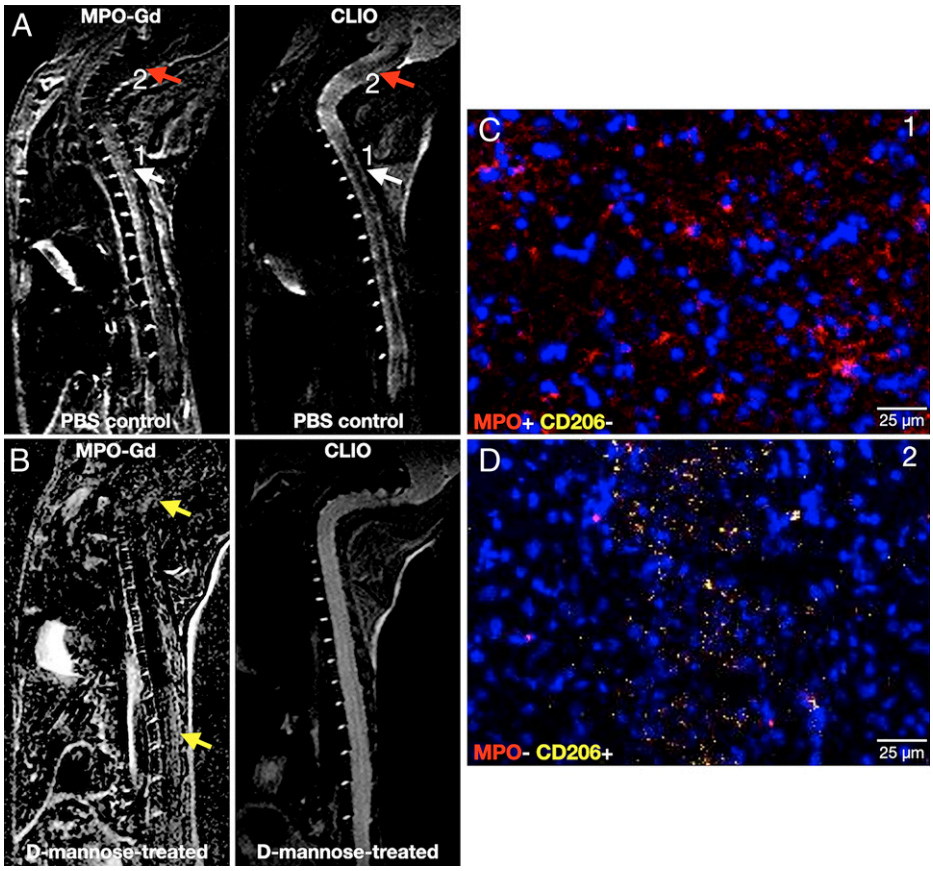

Fig. 4. Matching MPO-Gd and CLIO imaging of (*A*) PBS-control and (*B*) D-mannose–treated EAE animals. In *A*, MPO-Gd$^+$ lesions with matched CLIO$^+$ lesions (white arrows) represent M1-like phagocytes, corroborated by immunohistochemistry in *C*, where this area contained cells that expressed MPO but not CD206 (red = MPO, yellow = CD206, blue = DAPI). Lesions that were CLIO$^+$ only without corresponding MPO-Gd$^+$ signal (red arrow) represent M2-like phagocytes that expressed CD206 but virtually no MPO on immunohistochemistry (*D*). In *B*, D-mannose treatment markedly reduced CLIO signal in MPO-Gd$^+$ lesions (yellow arrows).

a 60-kg person with a dose of 2 to 4 g of D-mannose daily, or 33 to 66 mg/kg daily, and with a conversion factor of 12.3 from human dose to mouse dose (47), the equivalent dose of D-mannose for a mouse is 406 to 812 mg/kg. In this study, we treated the mice at a dose of 450 mg/kg, which is within the range of the clinical dose for UTI patients. For this experimental study, we chose intraperitoneal (IP) administration over the oral gavage route as the IP route is less stressful for these sick EAE animals. Pharmacokinetic studies have shown that at least 90% of ingested D-mannose is rapidly absorbed in the upper intestine into the blood (48), suggesting that the bioavailability of oral and IP administration may be similar. Nonetheless, future experiments and trials will be needed to determine the best route and dose to use for the treatment of neuroinflammatory diseases.

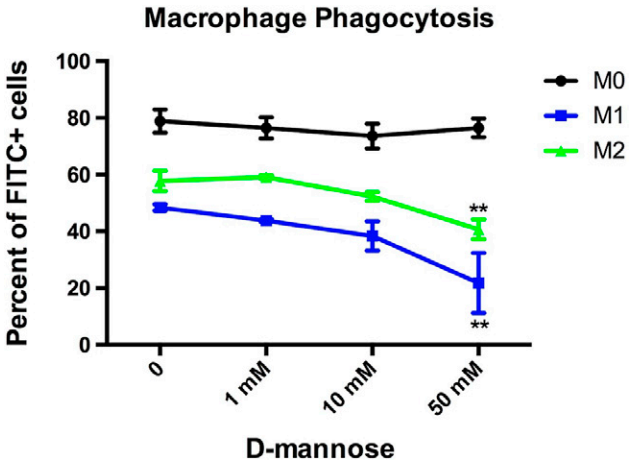

Fig. 5. In vitro MΦ phagocytosis in the presence of D-mannose. M1 and M2 MΦ demonstrated significantly decreased phagocytosis in a dose-dependent manner with D-mannose compared to M0 (**P = 0.0025 for M1, **P = 0.001 for M2).

In summary, we demonstrated that D-mannose treatment slowed clinical symptom progression, significantly reduced mortality, and beneficially modulated the inflammatory response in the CNS in a model of neuroinflammation. Our findings provide rationale for testing D-mannose as a potentially safe, low-cost treatment option for MS patients.

Methods

EAE Induction, Clinical Scoring, and Treatment. Animal experiments were approved by the local institutional animal care and use committee. All mice were maintained in a federally approved animal facility at Massachusetts General Hospital and allowed to acclimate for 1 wk prior to the start of the experiments. EAE was induced in 6- to 10-wk-old female C57BL/6 mice (The Jackson Laboratories) using myelin oligodendrocyte glycoprotein 35 to 55 peptide ($MOG_{35–55}$, AnaSpec) (200 μg/mouse) in complete Freund's adjuvant (Sigma) (50 μL/mouse) with *Mycobacterium tuberculosis* H37Ra (BD Difco) (800 μg/mouse). The $MOG_{35–55}$ emulsion was subcutaneously injected at bilateral axillary and inguinal sites. On day 0 and day 2 after induction, pertussis toxin (Sigma) (200 μg/mouse) was intravenously injected into the mice via tail vein. This method generates monophasic EAE with ascending flaccid paralysis

within 9 to 14 d after immunization (49). We induced EAE in 24 mice and divided them randomly into PBS-control (n = 12) and D-mannose–treated (n = 12) groups. Another 20 mice were induced with EAE and randomly divided into PBS-control, D-glucose–, D-fructose–, or D-galactose–treated groups (n = 5 per group). Three sham mice were induced with identical steps using PBS instead of MOG emulsion. Mice were checked for signs of EAE, and their weights and clinical scores were recorded daily by a researcher blinded to the treatment method. Clinical assessment for disease activity was performed using the Hooke's scoring scheme (50). Once the mouse dies, the clinical score was recorded as 5 for the rest of the study. We treated the mice with 450 mg/kg D-mannose (31) or the same volume of PBS intraperitoneally once a day from the day of induction. D-mannose powder (Sigma) was dissolved in PBS right before injection. Mice were observed and treated daily until day 19.

MR Imaging. MRI of the spinal cord was performed on an animal 4.7-T MR imaging unit with a mouse surface coil under respiration-monitored isoflurane anesthesia (Bruker). On day 15 after immunization, three mice from each group were randomly chosen regardless of clinical score by a researcher blinded to the treatment method for MR imaging. MPO-Gd was synthesized as previously described (19, 35). CLIO was kindly provided by Ralph Weissleder, Massachusetts General Hospital, Boston, MA. Precontrast enhanced T2-weighted imaging of the sagittal spinal cord was performed. At 24 h after the injection of CLIO (20 mg Fe/kg), postcontrast enhanced T2-weighted imaging was performed, followed by precontrast enhanced T1-weighted imaging. Postcontrast enhanced T1-weighted images were obtained sequentially every 15 min for 1 h after intravenous administration of MPO-Gd (0.3 mmol/kg). Two experienced authors, who were blinded to the clinical scores of the mice and treatment method, independently evaluated the MR images. Sagittal spinal cord imaging parameters for pre- and postcontrast enhanced T1-weighted imaging were as follows: repetition time (TR) = 700 ms, echo time (TE) = 14.0548 ms, matrix size 256 × 256, and slice thickness 0.5 mm. 12 sections were acquired. Imaging parameters for pre- and postcontrast enhanced T2-weighted imaging were as follows: TR = 4,000 ms, TE = 53.3333 ms, matrix size 256 × 256, slice thickness 0.5 mm. Twelve sections were acquired. Imaging parameters for T2 mapping were as follows: TR = 2,500 ms, TE = 8.30738, 16.6148, 24.9221, 33.2295, 41.5369, 49.8443, 58.1516, 66.459, 74.7664, 83.0738, 91.3811, 99.6885, 107.996, 116.303, 124.611, and 132.918 ms, matrix size 192 × 192, slice thickness 0.5 mm. Twelve sections were acquired. Mice were maintained in the same position for post-T2, T2 mapping, pre-T1 and post-T1 contrast-enhanced imaging. Postcontrast images for MPO-Gd were subtracted from the precontrast images to identify the lesions.

Leukocyte Isolation and Flow Cytometry. Mice were transcardially perfused with 20 to 30 mL ice-cold PBS. Spinal cords were collected and stored on ice in PBS before experiments. Leukocytes were extracted by density centrifugation over a discontinuous Percoll gradient (51). Briefly, spinal cord tissue was mechanically ground in a dounce homogenizer in 7 mL of 30% standard isotonic Percoll (SIP) solution (Percoll, GE Healthcare) and filtered through a 40-μm cell strainer (BD Biosciences). The 30% SIP/tissue homogenate was slowly laid under 2 mL of 70% SIP, followed by overlaying 2 mL PBS on top of the 30% SIP. The density gradient was centrifuged at 600 relative centrifugal force (rcf) for 25 min at 18 °C with brakes set to 2/2 to avoid interrupting the 30/70 SIP interface. After centrifugation, a thick myelin-containing layer at the top was discarded, and leukocytes at the 30/70 interface were collected. The cells were then counted and stained for flow cytometry. The following antibodies were used for flow cytometry: anti-CD90-PE (BD Biosciences); anti-NK1.1-PE (BD Biosciences); anti-B220-PE (BD Biosciences); anti-CD49b-PE, (BD Biosciences); anti-Ly6G-PE/Cy7 (BD Biosciences); anti-CD45.2-PB (BD Biosciences); anti-CD11b-APC/Cy7 (BD Biosciences); anti-Egr2-APC (Invitrogen); anti-MPO-biotin (Hycult Biotech). For intracellular staining of Egr2 and MPO, cells were fixed and permeabilized using Cytofix/Cytoperm (BD Bioscience) after staining for cell surface markers. Streptavidin-conjugated Brilliant Violet 605 secondary antibody (BioLegend) was used to label biotinylated anti-MPO. On flow cytometry, $CD11b^{+}CD45^{high}$ cells represented peripherally derived CNS-infiltrating MΦ or activated Mg that up-regulated CD45, while $CD11b^{+}CD45^{intermediate/low}$_$Ly6G^{-}$ represented resident Mg (39, 52–54). We applied the antibody for Egr2 (early growth response protein 2) to identify M2-like (antiinflammatory) MΦ/Mg (55, 56) and MPO to identify M1-like (proinflammatory) MΦ/Mg (57). Data were acquired with a flow cytometer (LSR II; BD Biosciences) and analyzed with dedicated software (FlowJo X 10.0; Tree Star).

Immunohistochemical Staining. Fresh frozen spinal cords were cut in serial cross-sections (10 μm thick). The sections were warmed for 30 min at room temperature (RT) and hydrated for 10 min with PBS. The slides were incubated in blocking buffer (1% of horse serum, 1% of bovine serum albumin, 1% of donkey serum, 0.3% Triton X-100 and 0.01% sodium azide in PBS) at RT for 1 h, followed by incubating in blocking buffer containing the primary antibody overnight at 4 °C. Primary antibodies were rabbit anti-MPO (1:500, Thermo Fisher, Cat. No. PA5-16672) and anti-CD206 biotin conjugated (1:100, Thermo Fisher, Cat. No. MA5-16869). On the second day, slides were rinsed with PBS and then incubated with secondary antibodies at RT for 1 h. Secondary antibodies were anti-rabbit Cy3 (1:800, Millipore Sigma, Cat. No. 3465436) and streptavidin Alexa Fluor 680 (1:400, Life Technology, Cat. No. 1395260). Sections were mounted in EMS glycerol mounting medium (Fisher Scientific, Cat. No. 17989-41) and DAPI.

In Vitro MΦ Phagocytosis. Bone marrow–derived MΦ were isolated and cultured (58) from 6- to 8-wk-old C57BL/6 mice. Red blood cells (RBCs) were lysed using RBC lysis buffer (BioLegend). Cells were counted and plated in six-well plates, suspending in MΦ differentiation medium (DMEM [Corning] with 30% L929-M-CSF-conditioned medium [LCM], 20% fetal bovine serum [FBS] [Atlanta Biologicals], and 20 μg/mL gentamicin [Sigma]). After culturing for 7 d in a humidified incubator with 5% CO_2 at 37 °C, the differentiation medium was replaced with activation medium to polarize M0 to M1 or M2 MΦ. Activation medium for M1 consisted of 20 ng/mL IFNγ and 100 ng/mL lipopolysaccharide, while activation medium for M2 consisted of 20 ng/mL IL-4. After 24 h of polarization, cells were ready to use. M0, M1, and M2 MΦ were incubated with different concentrations of D-mannose in DMEM (0 mM, 1 mM, 10 mM, and 50 mM) for 4 h at 37 °C, followed by adding FITC-tagged CLIO (FITC-CLIO, kindly provided by Ralph Weissleder) and incubating for 1.5 h (n = 3 for each condition). Similarly, M1 MΦ were incubated with different concentrations (0 mM, 1 mM, 10 mM, and 50 mM) of D-glucose, D-fructose, or D-galactose. Cells were then collected for flow cytometry. Data were acquired with a flow cytometer (LSR II; BD Biosciences) and analyzed using FlowJo X (v10.0; Tree Star). Cells that were not incubated with FITC-CLIO were used as negative controls (*SI Appendix*, Fig. S2*A*). All samples used the same gating strategy. The percentage of $FITC^{+}$ signal obtained from the histogram of each sample was used for statistical analysis.

Blinding and Randomization. For all animals in this study, the daily clinical scores and weights were recorded by a researcher blinded to the treatment method. The induced EAE mice were randomly divided into PBS-control and D-mannose–treated groups. The experiments were performed by researchers blinded to the treatment method and clinical scores. MR images were independently evaluated by two experienced researchers who were blinded to the treatment method.

Statistical Analysis. Results were reported as mean ± SE of measurement (SEM). Clinical severity between sham, PBS-control, and D-mannose treatment groups were analyzed using two-way ANOVA. Intergroup differences of in vitro MΦ phagocytosis were also analyzed using two-way ANOVA. Clinical severity between PBS-, D-glucose–, D-galactose–, and D-fructose–treated groups were evaluated using one-way ANOVA. Log rank (Mantel–Cox test) was applied to compare the survival rate between control and treatment group. For other intergroup comparisons, unpaired two-tailed t tests were used when no significant difference was found for the F test. Otherwise, a Mann–Whitney U test was applied. We chose the largest central slice of sagittal spinal cord for measuring the MPO^{+} and $CLIO^{+}$ lesion areas. We used ImageJ (Fiji) software (version 2.0.0-rc-67/1.52d) to measure the total lesion area for delayed (1 h) MPO-Gd–enhanced T1-weighted images and CLIO-enhanced T2-weighted images. To make lesions more obvious on MPO-Gd enhanced T1W images, we subtracted precontrast enhanced T1 images from the delayed postcontrast enhanced T1 images. All images had the same pixel size when importing into ImageJ (Fiji). We used Horos software (version 1.1.7) for image visualization. We used a GE Advanced Workstation for T2 mapping analysis (Functool 9.4.05). Three regions of interest within the $CLIO^{+}$ low signal lesions were chosen for each mouse to calculate the T2 values and the average values were used for the data analysis (n = 3 mice for both PBS-control and D-mannose–treated groups of mice). The robust regression and outlier removal (ROUT) test (Q = 1.0%) was used to identify outliers for flow cytometry data analysis. One outlier out of 10 mice was found in the D-mannose treatment group and was statistically excluded from the analysis. We used GraphPad Prism (v.6, GraphPad Software) for statistical analysis. $P < 0.05$ was considered statistically significant.

Data Availability. All study data are included in the article and/or supporting information.

ACKNOWLEDGMENTS. We thank Prof. Weissleder for providing CLIO. This work was supported by NIH Grant R01 NS103998, National Multiple Sclerosis Society Grants RG-1507-05486 and RG-1902-33633, and Shanghai Pujiang Program Grant 20PJ1402200.

1. D. Rotstein, X. Montalban, Reaching an evidence-based prognosis for personalized treatment of multiple sclerosis. *Nat. Rev. Neurol.* **15**, 287–300 (2019).
2. F. Chu *et al.*, The roles of macrophages and microglia in multiple sclerosis and experimental autoimmune encephalomyelitis. *J. Neuroimmunol.* **318**, 1–7 (2018).
3. E. Grajchen, J. J. A. Hendriks, J. F. J. Bogie, The physiology of foamy phagocytes in multiple sclerosis. *Acta Neuropathol. Commun.* **6**, 124 (2018).
4. E. J. McMahon, S. L. Bailey, C. V. Castenada, H. Waldner, S. D. Miller, Epitope spreading initiates in the CNS in two mouse models of multiple sclerosis. *Nat. Med.* **11**, 335–339 (2005).
5. L. Grau-López *et al.*, Myelin peptides in multiple sclerosis. *Autoimmun. Rev.* **8**, 650–653 (2009).
6. B. F. Popescu, I. Pirko, C. F. Lucchinetti, Pathology of multiple sclerosis: Where do we stand? *Continuum (Minneap. Minn.)* **19** (4 Multiple Sclerosis), 901–921 (2013).
7. I. Nikić *et al.*, A reversible form of axon damage in experimental autoimmune encephalomyelitis and multiple sclerosis. *Nat. Med.* **17**, 495–499 (2011).
8. P. K. Stys, G. W. Zamponi, J. van Minnen, J. J. Geurts, Will the real multiple sclerosis please stand up? *Nat. Rev. Neurosci.* **13**, 507–514 (2012).
9. L. A. Boven *et al.*, Myelin-laden macrophages are anti-inflammatory, consistent with foam cells in multiple sclerosis. *Brain* **129**, 517–526 (2006).
10. Y. Liu *et al.*, Suppression of microglial inflammatory activity by myelin phagocytosis: Role of p47-PHOX-mediated generation of reactive oxygen species. *J. Neurosci.* **26**, 12904–12913 (2006).
11. D. M. Hartung, D. N. Bourdette, S. M. Ahmed, R. H. Whitham, The cost of multiple sclerosis drugs in the US and the pharmaceutical industry: Too big to fail? *Neurology* **84**, 2185–2192 (2015).
12. B. Kranjčec, D. Papeš, S. Altarac, D-mannose powder for prophylaxis of recurrent urinary tract infections in women: A randomized clinical trial. *World J. Urol.* **32**, 79–84 (2014).
13. D. Porru *et al.*, Oral D-mannose in recurrent urinary tract infections in women: A pilot study. *J. Clin. Urol.* **7**, 208–213 (2014).
14. R. F. Rest, C. F. Farrell, F. L. Naids, Mannose inhibits the human neutrophil oxidative burst. *J. Leukoc. Biol.* **43**, 158–164 (1988).
15. X. L. Xu *et al.*, Mannose prevents lipopolysaccharide-induced acute lung injury in rats. *Inflamm. Res.* **57**, 104–110 (2008).
16. J. Kössi, J. Peltonen, T. Ekfors, J. Niinikoski, M. Laato, Effects of hexose sugars: Glucose, fructose, galactose and mannose on wound healing in the rat. *Eur. Surg. Res.* **31**, 74–82 (1999).
17. M. G. M. Freire *et al.*, Inflammatory responses induced in mice by lectin from *Talisia esculenta* seeds. *Toxicon* **42**, 275–280 (2003).
18. S. Torretta *et al.*, D-mannose suppresses macrophage IL-1β production. *Nat. Commun.* **11**, 6343 (2020).
19. J. W. Chen, M. O. Breckwoldt, E. Aikawa, G. Chiang, R. Weissleder, Myeloperoxidase-targeted imaging of active inflammatory lesions in murine experimental autoimmune encephalomyelitis. *Brain* **131**, 1123–1133 (2008).
20. A. Strzepa, K. A. Pritchard, B. N. Dittel, Myeloperoxidase: A new player in autoimmunity. *Cell. Immunol.* **317**, 1–8 (2017).
21. R. M. Nagra *et al.*, Immunohistochemical and genetic evidence of myeloperoxidase involvement in multiple sclerosis. *J. Neuroimmunol.* **78**, 97–107 (1997).
22. E. Gray, T. L. Thomas, S. Betmouni, N. Scolding, S. Love, Elevated myeloperoxidase activity in white matter in multiple sclerosis. *Neurosci. Lett.* **444**, 195–198 (2008).
23. E. Gray, T. L. Thomas, S. Betmouni, N. Scolding, S. Love, Elevated activity and microglial expression of myeloperoxidase in demyelinated cerebral cortex in multiple sclerosis. *Brain Pathol.* **18**, 86–95 (2008).
24. D. Lau *et al.*, Myeloperoxidase mediates neutrophil activation by association with CD11b/CD18 integrins. *Proc. Natl. Acad. Sci. U.S.A.* **102**, 431–436 (2005).
25. C. Y. Chang *et al.*, Dual functionality of myeloperoxidase in rotenone-exposed brain-resident immune cells. *Am. J. Pathol.* **179**, 964–979 (2011).
26. D. L. Lefkowitz, S. S. Lefkowitz, Microglia and myeloperoxidase: A deadly partnership in neurodegenerative disease. *Free Radic. Biol. Med.* **45**, 726–731 (2008).
27. J. P. Eiserich *et al.*, Myeloperoxidase, a leukocyte-derived vascular NO oxidase. *Science* **296**, 2391–2394 (2002).
28. D. L. Lefkowitz *et al.*, Neutrophilic myeloperoxidase-macrophage interactions perpetuate chronic inflammation associated with experimental arthritis. *Clin. Immunol.* **91**, 145–155 (1999).
29. K. Grattendick *et al.*, Alveolar macrophage activation by myeloperoxidase: A model for exacerbation of lung inflammation. *Am. J. Respir. Cell Mol. Biol.* **26**, 716–722 (2002).
30. J. A. Lincoln *et al.*, Exogenous myeloperoxidase enhances bacterial phagocytosis and intracellular killing by macrophages. *Infect. Immun.* **63**, 3042–3047 (1995).
31. X. Xu *et al.*, Involvement of mannose receptor in the preventive effects of mannose in lipopolysaccharide-induced acute lung injury. *Eur. J. Pharmacol.* **641**, 229–237 (2010).
32. M. P. Gelderman *et al.*, Perpetuation of inflammation associated with experimental arthritis: The role of macrophage activation by neutrophilic myeloperoxidase. *Mediators Inflamm.* **7**, 381–389 (1998).
33. A. J. Cuter, K. A. Davies, "Antigen clearance" in *Encyclopedia of Immunology.* P. J. Delves, I. M. Roitt, Eds. (Academic Press, ed. 2, 1998), pp. 182–188.
34. B. Pulli *et al.*, Multiple sclerosis: Myeloperoxidase immunoradiology improves detection of acute and chronic disease in experimental model. *Radiology* **275**, 480–489 (2015).
35. J. W. Chen, M. Querol Sans, A. Bogdanov Jr., R. Weissleder, Imaging of myeloperoxidase in mice by using novel amplifiable paramagnetic substrates. *Radiology* **240**, 473–481 (2006).
36. R. Forghani *et al.*, Demyelinating diseases: Myeloperoxidase as an imaging biomarker and therapeutic target. *Radiology* **263**, 451–460 (2012).
37. R. Weissleder, M. Nahrendorf, M. J. Pittet, Imaging macrophages with nanoparticles. *Nat. Mater.* **13**, 125–138 (2014).
38. M. Settles *et al.*, Different capacity of monocyte subsets to phagocytose iron-oxide nanoparticles. *PLoS One* **6**, e25197 (2011).
39. K. Kirschbaum *et al.*, In vivo nanoparticle imaging of innate immune cells can serve as a marker of disease severity in a model of multiple sclerosis. *Proc. Natl. Acad. Sci. U.S.A.* **113**, 13227–13232 (2016).
40. L. East, C. M. Isacke, The mannose receptor family. *Biochim. Biophys. Acta* **1572**, 364–386 (2002).
41. L. Martinez-Pomares, The mannose receptor. *J. Leukoc. Biol.* **92**, 1177–1186 (2012).
42. S. E. Pontow, V. Kery, P. D. Stahl, Mannose receptor. *Int. Rev. Cytol.* **137B**, 221–244 (1992).
43. G. W. Kreutzberg, Microglia: A sensor for pathological events in the CNS. *Trends Neurosci.* **19**, 312–318 (1996).
44. B. Hemmer, M. Kerschensteiner, T. Korn, Role of the innate and adaptive immune responses in the course of multiple sclerosis. *Lancet Neurol.* **14**, 406–419 (2015).
45. E. N. Benveniste, Role of macrophages/microglia in multiple sclerosis and experimental allergic encephalomyelitis. *J. Mol. Med. (Berl.)* **75**, 165–173 (1997).
46. C. A. Hoppe, Y. C. Lee, Stimulation of mannose-binding activity in the rabbit alveolar macrophage by simple sugars. *J. Biol. Chem.* **257**, 12831–12834 (1982).
47. FDA, Guidance for Industry. Estimating the maximum safe starting dose in initial clinical trials for therapeutics in adult healthy volunteers. https://www.fda.gov/media/72309/download (Accessed 1 Aug 2021).
48. F. Scaglione, U. M. Musazzi, P. Minghetti, Considerations on D-mannose mechanism of action and consequent classification of marketed healthcare products. *Front. Pharmacol.* **12**, 636377 (2021).
49. S. Bittner, A. M. Afzali, H. Wiendl, S. G. Meuth, Myelin oligodendrocyte glycoprotein (MOG35-55) induced experimental autoimmune encephalomyelitis (EAE) in C57BL/6 mice. *J. Vis. Exp.* **86**, 51275 (2014).
50. Mouse EAE Scoring. https://hookelabs.com/services/cro/eae/MouseEAEscoring.html. Accessed 1 Aug 2021.
51. P. A. Pino, A. E. Cardona, Isolation of brain and spinal cord mononuclear cells using percoll gradients. *J. Vis. Exp.* **48**, 2348 (2011).
52. I. D. Vainchtein *et al.*, In acute experimental autoimmune encephalomyelitis, infiltrating macrophages are immune activated, whereas microglia remain immune suppressed. *Glia* **62**, 1724–1735 (2014).
53. S. Rangaraju *et al.*, Differential phagocytic properties of $CD45^{low}$ microglia and $CD45^{high}$ brain mononuclear phagocytes-activation and age-related effects. *Front. Immunol.* **9**, 405 (2018).
54. A. Crotti, R. M. Ransohoff, Microglial physiology and pathophysiology: Insights from genome-wide transcriptional profiling. *Immunity* **44**, 505–515 (2016).
55. K. A. Jablonski *et al.*, Novel markers to delineate murine M1 and M2 macrophages. *PLoS One* **10**, e0145342 (2015).
56. D. C. Cockrell *et al.*, Robust growth of avirulent phase II *Coxiella burnetii* in bone marrow-derived murine macrophages. *PLoS One* **12**, e0173528 (2017).
57. S. Sugiyama *et al.*, Macrophage myeloperoxidase regulation by granulocyte macrophage colony-stimulating factor in human atherosclerosis and implications in acute coronary syndromes. *Am. J. Pathol.* **158**, 879–891 (2001).
58. I. Pineda-Torra, M. Gage, A. de Juan, O. M. Pello, Isolation, culture, and polarization of murine bone marrow-derived and peritoneal macrophages. *Methods Mol. Biol.* **1339**, 101–109 (2015).